Int. J. Electrochem. Sci., 17 **(2022)** Article Number: 220748, doi: 10.20964/2022.07.34

International Journal of
ELECTROCHEMICAL
SCIENCE
www.electrochemsci.org

Imidazolidiny Urea as a Potential Corrosion Inhibitor for Mild Steel in HCl Medium: Experimental and Density-Functional Based Tight-Binding Methods

Lei Guo[1,3], *Yuzhou Luo*[2,*], *Yue Huang*[4], *Wenjie Yang*[5], *Xingwen Zheng*[6], *Yuanhua Lin*[1,*], *Riadh Marzouki*[7,8]

[1] State Key Laboratory of Oil and Gas Reservoir Geology and Exploitation, Southwest Petroleum University, Chengdu 610500, China
[2] Business School, Guilin University of Technology, Guilin 541000, China
[3] School of Material and Chemical Engineering, Tongren University, Tongren 554300, China
[4] College of Materials and Metallurgy, Guizhou University, Guiyang 550025, China
[5] Bohai Shipyard Group Corporation Limited, Huludao 125004, China
[6] Key Laboratory of Material Corrosion and Protection of Sichuan Province, Zigong 643000, China
[7] Chemistry Department, College of Science, King Khalid University, Abha 61413, Saudi Arabia
[8] Chemistry Department, Faculty of Sciences, University of Sfax, 1171 Sfax 3000, Tunisia
[*]E-mail: luoyuzhouluo@126.com, yhlin28@163.com

Received: 12 March 2022 / *Accepted:* 2 May 2022 / *Published:* 6 June 2022

This work focuses on the investigation of the inhibitory activity of imidazolidiny urea (IU) on mild steel in acidic environment by electrochemical and scanning electron microscopy (SEM) methods. The obtained results showed that adding IU to the corrosive medium significantly slows down the corrosion process, and the maximum inhibition efficiency can achieve 95% when the inhibitor concentration is 28 mM. The potentiodynamic polarization approach evidenced that IU is a mixed-type inhibitor and its adhesion on the substrate surface obeyed Langmuir adsorption isotherm. The SEM-EDS results show that a thin barrier film formed on the steel surface, which isolated the metal substrate from corrosive solution and then decoupled the cathodic & anodic corrosion processes. In addition, density-functional based tight-binding (DFTB) calculations were conducted to validate the inhibition mechanism. All obtained results ensure that the IU can control the corrosion process. This research provides a new candidate for environmental friendly corrosion inhibitors which has wide application prospect in the industry.

Keywords: Corrosion inhibitor, Mild steel, Imidazolidiny urea, Electrochemistry, DFTB calculations

1. INTRODUCTION

Mild steel is a valuable construction material used in various industries on account of its low cost and outstanding mechanical properties. Nevertheless, corrosion can cause severe economic damage to

steel infrastructure, and this issue has received increasing attention in recent decades [1]. Many experiments have confirmed that using corrosion inhibitor is an effective means to suppress the degradation of steel in corrosive medium [2, 3]. Organic compounds containing N, O, and S heteroatoms were found to be effective corrosion inhibitors for metals. This is because they have the ability to form strong coordination bond with metal atoms, and the inhibition efficiency is normally in the order of O < N < S [4].

Up to now, a range of compounds such as azoles, amino acids, Schiff base, ionic liquids, and plant extracts have been proved to exhibit excellent corrosion inhibition performance [5-7]. Some common electron-rich groups often serve as adsorption centres, for example, polar functional substituents (−NH_2, −OH, −NHMe, −OMe), multiple bonds (C≡N, N=O, C=O, C=S, N=N), and aromatic rings [8]. Researchers also found that there exists certain structure-activity relationships between the inhibition efficiency and molecular structure [9, 10]. However, due to the complexity of the real corrosion environment, it is still difficult to accurately predict the inhibition performance only from a theoretical perspective [11]. In numerous literatures related to inhibitor calculations during the past years, most of them have either concerned on a straightforward correlation between molecular electronic descriptors and the inhibition performance and/or on conventional force-field based molecular dynamics simulations. However, the former cannot always explain inhibition effectiveness and offer little physical insight, while the latter cannot provide covalent bonding information [12]. Therefore, some semi-empirical algorithms are widely developed. Thereinto, based on the Kohn-Sham total energy in density functional theory with respect to charge density fluctuations, the DFTB method uses a second-order expansion, which allows to perform fast & efficient simulations for large systems [13].

In recent years, with the increasingly strict environmental protection regulations and the needs of sustainable development, the development of low toxicity and environment-friendly corrosion inhibitors remains a hot research field. The current study aims to investigate the inhibitive and adsorption properties of an antimicrobial preservative, namely IU, on the surface of mild steel using electrochemical techniques, surface analysis methods, and DFTB calculations.

2. EXPERIMENTAL

2.1. Materials and reagents

Q235 mild steel with the following weight percentage chemical composition was employed as working electrode: C 0.102%, Mn 1.06%, Si 0.34 %, P 0.018%, S 0.17%, Ni 0.18 %, and the rest of Fe. As cylindrical, the specimens were purchased from Shengxin Technology (Shandong) Co., Ltd. Electrochemical experiments were carried out on cylindrical specimens with a diameter of 1 cm. These specimen's surfaces were physically polished with silicon carbide paper ranging from 200 to 1200 grades, cleaned with distilled water, and degreased with acetone. The imidazolidiny urea and concentrated HCl (36~38%) were supplied by Kaiwei Chemical company. The corrosive environment employed in this investigation is 1 M HCl. The molecular structure of imidazolidiny urea, namely, 1,1'-methylenebis{3-[1-(hydroxymethyl)-2,5-dioxoimidazolidin-4-yl]urea} was given in Figure 1.

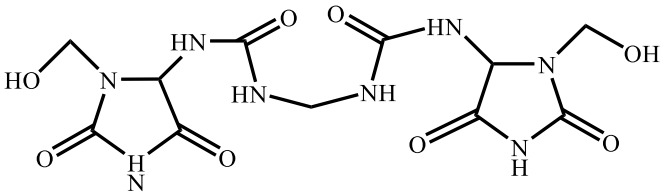

Figure 1. Chemical structure of imidazolidiny urea (IU).

2.2. Electrochemical experiments

In this work, the electrochemical measurements were carried out through the CHI660E electrochemical workstation of Shanghai Chenhua Instrument Co., Ltd. The reference electrode and counter electrode are saturated calomel electrode (SCE) and platinum sheet electrode, respectively. A Luggin capillary was placed near the working electrode to reduce ohmic contribution. The open circuit potential (OCP) of the corroding system was monitored for 1 h to ensure a steady-state condition. The adopted electrochemical impedance spectroscopy (EIS) experimental parameters were initial frequency = 100 kHz, final frequency = 10 mHz, amplitude signal = 10 mV acquiring 10 points/decade at OCP. The obtained EIS data were fitted by ZsimpWin 3.6 software. The potentiodynamic polarization (PDP) curves were carried out under the potential from −250 mV to +250 mV vs. OCP at a scan rate of 0.2 mV/s. Temperature was controlled using a water bath set at a constant temperature. For achieving precise results, all of the achievements were reported for three replicas of each sample.

2.3. Morphology analysis

Surface morphology of the mild steel samples before and after immersion in the test solutions was observed by the JEOL-JSM-7800F schottky field emission scanning electron microscope. For this aim, the prepared 1 cm × 1 cm samples were immersed in the prepared electrolytes for 6 h and their morphologies were then observed by the mentioned instrument.

2.4. Computational methodology

The computer-aided molecular simulations were carried out using the DFTB+ module implemented in Materials Studio software (BIOVIA, U.S.) [14]. The self-consistent-charge DFTB algorithm is based on atomic basis functions and tight-binding approximations of the Hamiltonian, and can be applied to periodic and cluster computational tasks. The interactions between IU molecule and mild steel surface were modeled in a simulation box (17.3 Å×17.3 Å×26.1 $Å^3$) with periodic boundary conditions. In previous work, we found that Fe(110) is a close-packed surface and has a stable structure, thus it was chosen as the simulated substrate [15]. A four-layer 7×7 supercell (the bottom two layers were constrained) with 25 Å vacuum slab was used to represent the bulk metal. The orbital occupation was subjected to a thermal smearing value (0.005 Ha) to accelerate convergence. In all DFTB calculations, the trans3d Slater-Koster was used to describe the interaction of atoms. The convergence

thresholds for energy, force, and displacement were set as 0.02 kcal/mol, 0.1 kcal/mol/Å, and 0.001 Å, respectively.

3. RESULTS AND DISCUSSION

3.1. OCP and PDP analysis

The kinetics of electrochemical processes of corrosion and inhibition processes were investigated by PDP analysis. Figure 2a indicated the OCP curves of corrosion and inhibited solution. It is clear that the OCP decreased slowly in the corrosion solution, confirming that the metal salts and other deposits were formed in the corrosion processes, and the metal surface was seriously corroded. When the IU inhibitor was added in the corrosion solution, the OCP was changed to more negative areas, confirming that the studied IU inhibitor formed a protective film, which are more stable on the metal surface.

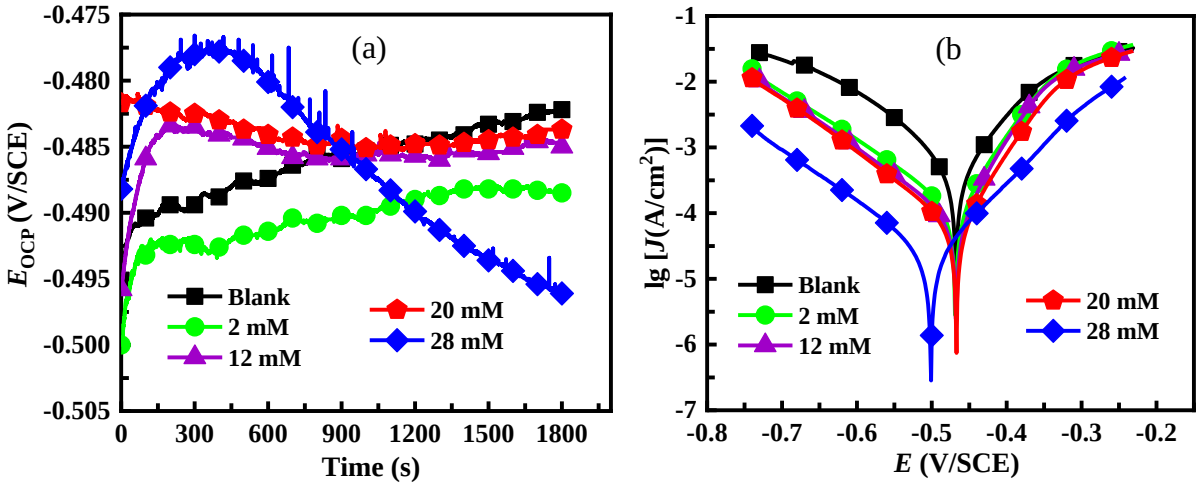

Figure 2. (a) OCP variations and (b) polarization curves for the mild steel samples in the uninhibited and IU inhibited 1 M HCl solutions.

Potentiodynamic polarization curves for the inhibitor absence and presence of acidic solution were indicated in Figure 2b. Actually, the aggressive chloride ions attack to the metal surface and form the active ions on the metal surface. As a result, the metal surface was seriously destroyed and corrosion current density was dramatically increased. After adding IU inhibitor, the potentiodynamic polarization curves were shifted to more lower corrosion current density regions. This is due to the inhibitor largely blocked the number of active corrosive ions. As a consequence, the polarization of solution was decreased. The corrosive chloride and hydrogen ions on the metal surface were significantly neutralised. The carbonyl, amine, and hydroxyl functional groups of IU were responsible for the inhibition effect. The π-electrons and delocalised electrons can be shared to active iron ions to form the covalent bonds [16]. The obtained PDP curves were employed to estimate the data of polarization parameters such as the corrosion current density (I_{corr}), cathodic and anodic Tafel slopes (β_c and β_a), and corrosion potential (E_{corr}). The amount of corrosion current densities in the uninhibited and inhibited solution were uesd to measure the inhibition efficiency (η_{PDP}) [17]:

$$\eta_{PDP}\% = \frac{I_{corr,0} - I_{corr}}{I_{corr,0}} \times 100 \quad (1)$$

where $I_{corr,\,0}$ and I_{corr} represent corrosion current densities without and with IU, respectively.

The obtained data was represented in Table 1. It is noted that the potential difference between the corrosive and inhibited medium shows the inhibitor type. Less than 85 mV is responsible for the mixed-type and over 85 mV shows the anodic or cathodic type [18]. It should be underlined fact in the obtained data that the potential difference of IU inhibitor was around 10~30 mV, showing that the investigated inhibitor was mixed type. The shifts of β_a and β_c imply that IU inhibits the anodic reaction as well as the cathodic process of steel electrode in HCl solution at the same time. As observed, the I_{corr} was 506 μA/cm^2 for the blank solution. In comparison, the value of corrosion current density was dramatically decreased to 24.66 μA/cm^2 when the IU concentration is 28 mM, with a high η_{PDP} value of 95%.

Table 1. Potentiodynamic polarization results for the corrosive and inhibited 1 M HCl solution.

C (mM)	E_{corr} (V/SCE)	i_{corr} (μA/cm^2)	β_c (mV/dec)	β_a (mV/dec)	ϑ	η_{PDP} (%)
Blank	−0.468	506.0	−118	91	/	/
2	−0.469	129.6	−131	65	0.74	74
12	−0.467	82.43	−121	55	0.83	83
20	−0.467	65.82	−119	61	0.86	86
28	−0.501	24.66	−120	89	0.95	95

3.2. EIS measurement

Electrochemical impedance spectroscopy is a powerful technique used for the analysis of interfacial properties related to corrosion events occurring at the electrode surface. Therefore, the corrosion and inhibition processes were also investigated by the EIS analysis in this work. The obtained Nyquist plots were displayed in Figure 3a. It is noted that all obtained Nyquist curves were depressed semirings, showing that the charge-transfer mechanism controls the reaction processes [19]. Figure 3b displayed the Bode and phase angle plots for mild steel electrode in the inhibitor-free and inhibitor-contained solutions at the various concentrations. It is notable that the Bode and phase angle graphs have one time constant with a single maximum at the intermediate frequency, demonstrating that corrosion and inhibition needed relaxation processes on the working electrode. The shape of Bode and phase angle plots depends on the change of inhibitor concentration. The value of impedance modulus (|Z|) increases with increasing inhibitor concentration, which indicates that the adsorption of IU inhibits the corrosion of steel in HCl solution.

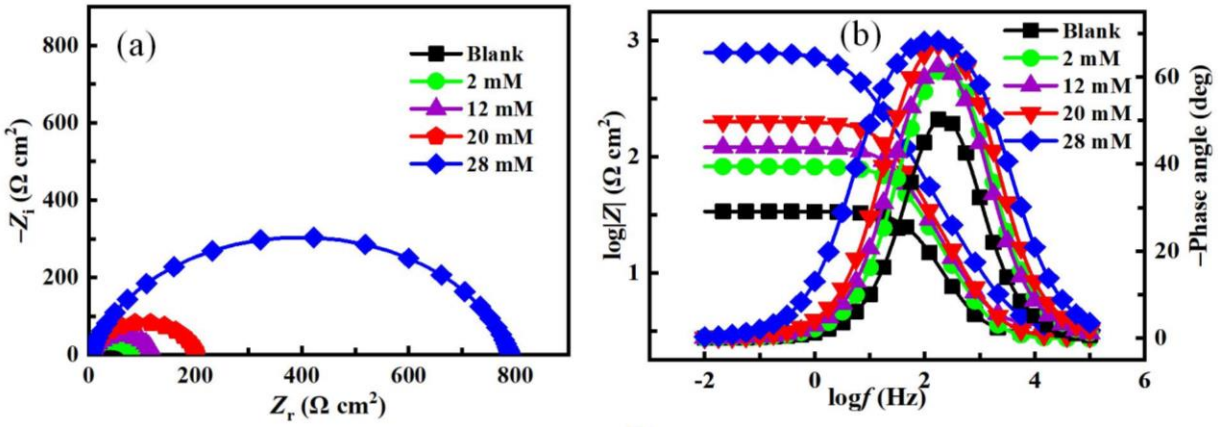

Figure 3. (a) Nyquist and (b) Bode plots for mild steel in 1 M HCl before and after the addition of different concentrations of IU.

A classical equivalent circuit, as shown in Figure 4, was used to estimate the EIS kinetic parameters. This equivalent circuit contains the constant phase element (CPE), the charge transfer resistance (R_{ct}), and the solution resistance (R_s). CPE is usually used to replace ideal capacitor to compensate the deviation from the ideal dielectric behavior caused by the inhomogeneous nature of electrode surface. The impedance function of CPE can be described by the equation [20, 21]:

$$Z_{CPE} = Y_0^{-1}\left(j\omega\right)^{-n} \tag{2}$$

where Y_0 is a proportional factor, ω is the angular frequency, j represents the imaginary unit, and n is the phase shift, which is equal to 1, 0, and −1 represents the pure capacitor, resistor, and inductor, respectively. The double layer capacitance (C_{dl}) and inhibition efficiency (η_{EIS}) were obtained by the following formulas [22]:

$$C_{dl} = Y_0\left(\omega_{max}\right)^{n-1} = Y_0\left(2\pi f_{Z_{im-Max}}\right)^{n-1} \tag{3}$$

$$\eta_{EIS}\% = \frac{R_{ct} - R_{ct,0}}{R_{ct}} \times 100 \tag{4}$$

where ω_{max} delegates the frequency at which the imaginary impedance has the highest value. $R_{ct,0}$ and R_{ct} are the charge transfer resistance without and with IU inhibitor, respectively.

It is clear from Table 2 that the chi-square values (χ^2) were very low in all cases, signifying the high accurate of the equivalent circuit model. R_{ct} is 30.79 Ω cm^2 in the blank solution, but R_{ct} increases significantly after using IU additive. The inhibition efficiency attains a maximum value (95.73%) when inhibitor concentration is 28 mM. This is due to the formation of a protective film on the metal surface. This film can increase the charge transfer resistance. Nevertheless, the C_{dl} presents a decreasing trend, and the minimum C_{dl} was 39.6 μF/cm^2. This phenomenon can be explained by the Helmholtz model [23, 24]:

$$C_{dl} = \frac{\varepsilon^0 \varepsilon}{d} S \tag{5}$$

where ε and ε^0 are the local and air dielectric constant, respectively; S represents the surface area of mild steel electrode exposed to HCl solution; d stands for the thickness of the double layer. The decrease of C_{dl} was attributed to the adsorption of IU onto the steel/solution interface, and the inhibitor molecules

easily exchanged the pre-adsorbed water molecules on the metal surface, then the contact regions between the metal surface and solution reduced. The metal surface was effectively insulated in the presence of inhibitor, resulting in a decrease of the *S* and an increase of *d* values. Furthermore, the values of *n* for both the corrosion and inhibited solutions were close to one, indicating that the chosen electrode surface had a non-ideal capacitive nature due to the micro-districts on the surface and the unevenness of the electrode [25].

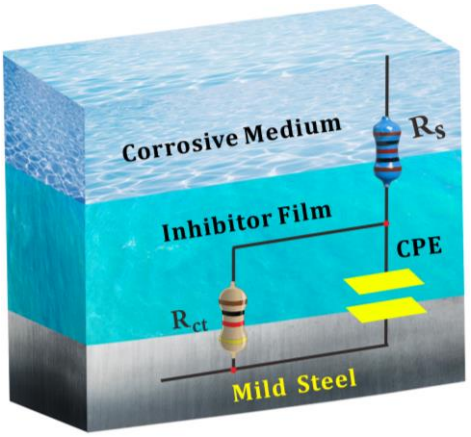

Figure 4. Equivalent circuit that models the metal/solution interface.

Table 2. The corrosion parameters of mild steel in 1 M HCl with and without IU inhibitor.

C (mM)	R_s (Ω cm^2)	CPE_{dl}		C_{dl} (μF cm^{-2})	R_{ct} (Ω cm^2)	χ^2 (10^{-3})	ϑ	η_{EIS} (%)
		Y_0 (10^{-6} S s^n cm^{-2})	n					
Blank	2.987	149.8	0.9139	90.24	30.79	3.65	/	/
2	2.697	93.84	0.9068	56.72	79.58	3.673	0.590	58.95
12	3.486	85.97	0.9008	51.81	117.2	2.945	0.720	72.01
20	2.794	75.16	0.8932	45.44	198.1	3.833	0.832	83.19
28	3.154	69.75	0.8368	39.60	787.5	3.787	0.957	95.73

3.3. Adsorption isotherm

The analysis of the adsorption behavior is important to describe the corrosion inhibition mechanism. The adsorption type and nature of the inhibitor molecule on the steel surface is well elucidated by the Langmuir adsorption isotherm, which is expressed by the following expression [26, 27]:

$$\frac{C}{\theta} = \frac{1}{K_{ads}} + C \tag{6}$$

where C is the inhibitor concentration, θ denotes the surface coverage, and K_{ads} represents the equilibrium adsorption constant. The θ values were selected from the EIS measurement as mentioned in Table 2. As shown in Figure 5, the correlation coefficient R^2 are close to unity, and the achieved high

value of K_{ads} confirmed that IU possesses strong adsorption capability on the steel surface. The values of Gibbs free energy (ΔG^0_{ads}) were measured using the following formula [28]:

$$\Delta G_{ads} = -RT \ln(55.5 K_{ads}) \quad (7)$$

where R is the universal gas constant and 55.5 is the molar concentration of water molecules. It is generally believed that the value of ΔG^0_{ads} less than −40 kJ/mol means the adsorption of corrosion inhibitor on the metal surface is chemisorption, while the ΔG^0_{ads} value greater than −20 kJ/mol indicates physisorption mainly occurs [29]. In our case, the value of ΔG^0_{ads} is between −40 and −20 kJ/mol, implying that the adsorption of IU on mild steel surface is a spontaneous process and belongs to the mixed adsorption involving both physical and chemical process. In other words, the IU inhibitor influences both the cathodic and anodic activities.

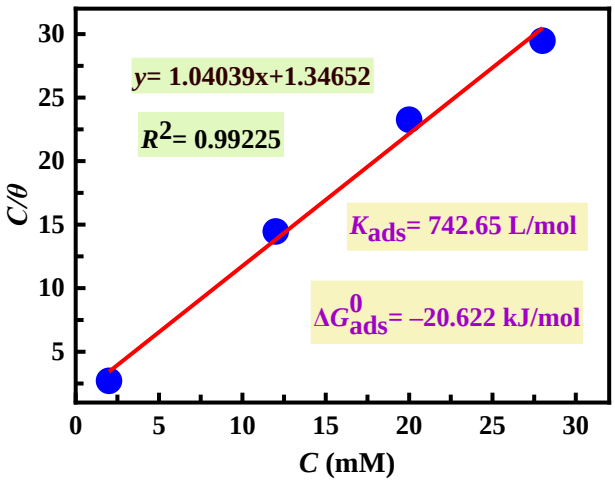

Figure 5. Langmuir adsorption plot of imidazolidiny urea inhibitor on the mild steel surface in 1 M HCl solution.

3.4. Surface morphological studies

SEM was used to observe the surface morphology of steel samples immersed in the test solution for 6 h, and the results are shown in Figure 6. Obviously, the polished mild steel surface is clean and very smooth. However, the mild steel surface under the blank circumstance is seriously damaged and corroded. As a result of corrosion destruction, the corrosion products of chlorides and oxides were formed on the metal surface. In comparison, the metal surface was relatively smooth in the inhibited case. According to the EDS results, the N and O elements was observed when the steel was treated with IU inhibitor, which confirms the adsorption of the IU molecule as a protective layer on the metal surface. It is also clear that the composition of chloride is relatively high in corrosive solutions, but the composition is lower in the inhibited solution. Therefore, the high concentration of chloride ions is responsible for the high corrosion while its low concentration is attributed to a rise in corrosion protection.

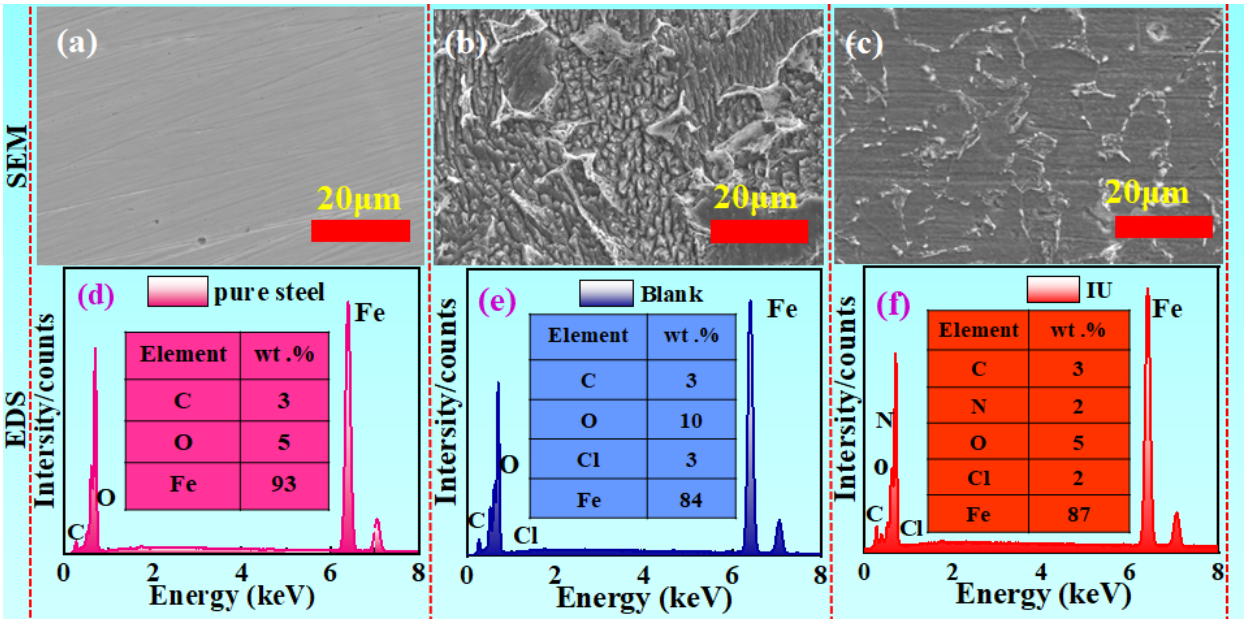

Figure 6. SEM-EDS results of mild steel under different conditions: (a, d) polished mild steel, (b, e) immersed in blank solution, (c, f) immersed in 1 M HCl medium containing 28 mM IU.

3.5. DFTB calculations

In order to get more bonding information between the IU molecule and Fe(110) surface, DFTB based geometric optimization was carried out. The most stable adsorption equilibrium configurations of IU on Fe(110) are visualized in Figure 7. As we can see, the IU molecule adheres to the steel substrate in almost flat orientation to maximize surface contact, creating a strong interaction between adsorbate and substrate. The representative Fe−N and Fe−O bond lengths are 2.865 Å and 2.755 Å, respectively. Under such circumstances, crucial covalent bonds can generate through sharing π electrons of the imidazol ring as well as lone pair electrons of the N, O atoms with Fe 3d orbitals.

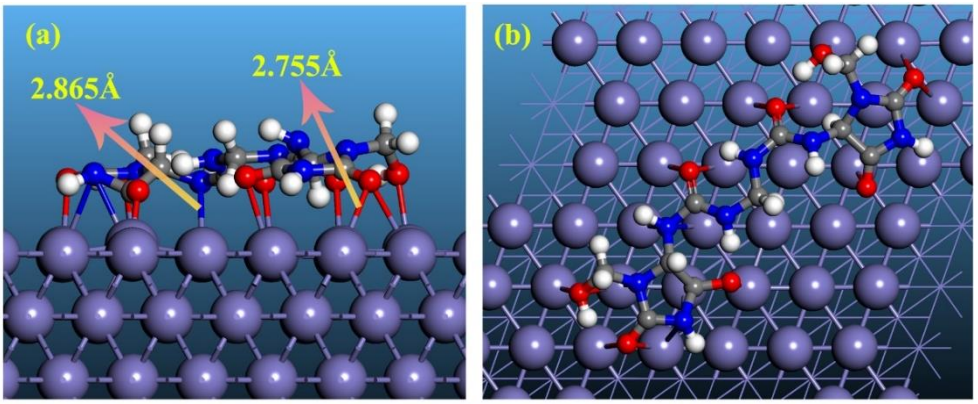

Figure 7. Side and top views of the equilibrium adsorption configurations of IU on Fe(110) surface.

In addition, a quantitative determination of the inhibitor's interaction strength with the Fe-surface was performed using the adsorption energy (E_{ads}) [30]:

$$E_{ads} = E_{IU/slab} - (E_{IU} + E_{slab}) \quad (8)$$

where $E_{IU/slab}$ is total energy of the adsorption system, E_{IU} represents the energy of isolated IU molecule, E_{slab} stands for the energy of the Fe(110) slab. In this work, the calculated E_{ads} value of IU inhibitor is −3.49 eV. It can be seen that the adsorption energy is negative and thus spontaneous adsorption can be expected. Normally, the charge density difference ($\Delta\rho$) may be used to assess the binding type and charge transfer of an adsorbed system. The isosurface plots of $\Delta\rho$ were obtained by subtracting the charge densities of individual isolated molecules (ρ_{ads}) and Fe(110) (ρ_{surf}) surface from the charge density of the whole adsorption configuration ($\rho_{surf+ads}$) [31, 32]:

$$\Delta\rho = \rho_{surf+ads} - (\rho_{ads} + \rho_{surf}) \quad (9)$$

The obtained $\Delta\rho(r)$ plot for the optimized adsorption geometry is depicted in Figure 8a. Wherein, red areas represent electron accumulation and blue regions mean electron depletion, respectively. It is readily seen that there exists electron accumulation on the Fe surface and electron depletion of IU molecule, suggesting that the functionalization of IU is realized by forming chemical bonds between the own active atoms and iron surface.

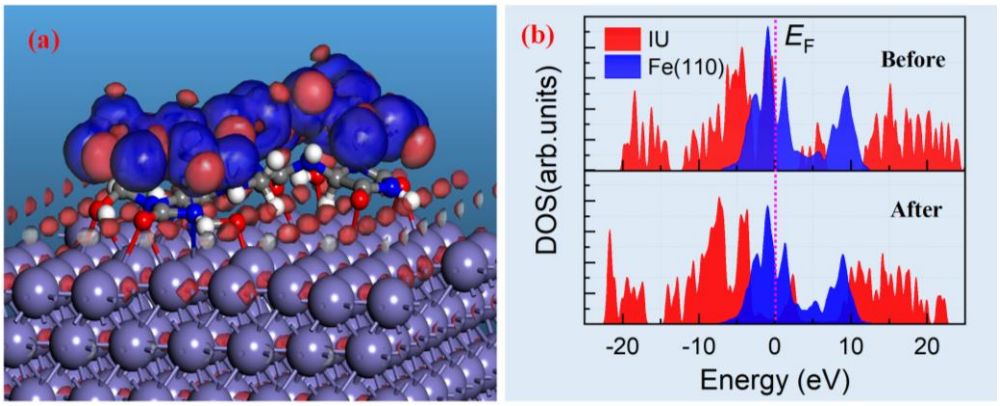

Figure 8. (a) Electron density difference plots and (b) projected density of states for the IU/Fe(110) adsorption system.

Besides, the density of states (DOS) distributions of the IU inhibitor molecule and Fe(110) surface before and after the adsorption were also explored. As revealed in Figure 8b, a discrete discontinuous energy level structure can be found in the DOS of IU before adsorption. After the IU molecule adsorbed on Fe(110) surface, its DOS plots exhibit a continuous energy band structure, which overlaps with the open 3*d* valence electron orbitals of Fe atoms near the Fermi level (E_F). In other perspective, the DOS of IU is absolutely broadened after adsorption, which can be attributed to the strong hybridization between the inhibitor and metal surface [33]. The above results reveal that the excellent corrosion inhibition performance of IU attributes to the orbital hybridizations at the solution/metal interface.

3.6. Inhibition and adsorption mechanism

In this section, we try to give a comprehensive clarification for the anticorrosive mechanism of IU in acid solution. As we know, the anodic dissolution of mild steel in HCl medium usually follows the following reactions [34]:

$$Fe + Cl^- \rightarrow (FeCl^-)_{ads} \quad (10)$$

$$(FeCl^-)_{ads} \rightarrow (FeCl)_{ads} + e^- \quad (11)$$

$$(FeCl)_{ads} \rightarrow (FeCl^+) + e^- \quad (12)$$

$$FeCl^+ \rightarrow Fe^{2+} + Cl^- \quad (13)$$

As displayed in Figure 9, in the blank solution, the corrosive species (H_3O^+, Cl^-) can access to mild steel substrate easily, and then bring about severe corrosion of mild steel. In this case, the anode releases the electrons, and the involving electrons flowed to the cathode, resulting in the occurring of discharge reaction [35]:

$$Fe + H^+ \rightarrow (FeH^+)_{ads} \quad (14)$$

$$(FeH^+)_{ads} + e^- \rightarrow (FeH)_{ads} \quad (15)$$

$$(FeH)_{ads} + H^+ + e^- \rightarrow Fe + H_2 \quad (16)$$

After the above-mentioned series of steps, the mild steel would be gradually degradated due to the pitting corrosion. But after using IU inhibitor, a thin [Fe(0)IU] self-assembled barrier film can be formed on steel surface:

$$Fe(0) + IU \rightarrow [Fe(0)IU] \quad (17)$$

Consequently, by preventing the diffusion of corrosion-causing ions, the corrosion process is effectively suppressed. We can conclude that that the addition of the IU inhibitor decouples the anodic oxidation of the steel as well as the reduction of hydronium ions.

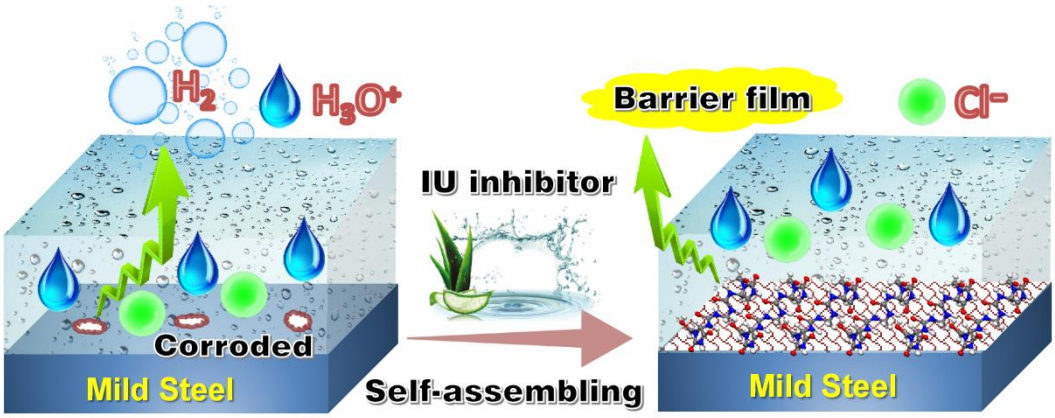

Figure 9. Proposed adsorption and inhibition mechanism of IU for mild steel in HCl medium.

4. CONCLUSIONS

In summary, IU was introduced as an effective decoupled inhibitor for mild steel corrosion in HCl medium. The electrochemical experiment results suggested that the inhibition efficiency for IU can

reach 95% at 28 mM at 298 K. EIS parameters for mild steel in 1 M HCl with and without IU show that the value of R_{ct} and inhibition efficiency increase as the concentration of inhibitor increases. Similarly, PDP analysis revealed the mixed type adsorption behaviour of IU molecules on mils steel surface. The SEM and EDX analysis mainly show the formation and composition of the protective layer of IU on the metal surface. Finally, the DFTB based computational analysis reveals that the electron-donating and electron-accepting properties are correlated with the inhibition performance.

ACKNOWLEDGMENTS
Riadh Marzouki extends the appreciation to the Deanship of Scientific Research at King Khalid University for funding this work through General Research Project under grant number (GRP. 273/40). This work was partly sponsored by the National Natural Science Foundation of China (21706195, 52074232), the Science and Technology Program of Guizhou Province (QKHPTRC[2021]5643, QKHZK[2022]555), the Foundation of the Department of Education of Guizhou province (QJHKY[2020]067), and the Opening Project of Sichuan University of Science and Engineering, Material Corrosion and Protection Key Laboratory of Sichuan province (2020CL06).

References

1. H. K. Worner, *Anti-Corros. Method. M.*, 3 (1956) 289.
2. R. Aslam, G. Serdaroglu, S. Zehra, D. Kumar Verma, J. Aslam, L. Guo, C. Verma, E. E. Ebenso and M. A. Quraishi, *J. Mol. Liq.*, 348 (2022) 118373.
3. Y. Qiang, L. Guo, H. Li and X. Lan, *Chem. Eng. J.*, 406 (2021) 126863.
4. B. Usman, H. Maarof, H. H. Abdallah and M. Aziz, *Int. J. Electrochem. Sci.*, 10 (2015) 3223.
5. Y. L. Kobzar and K. Fatyeyeva, *Chem. Eng. J.*, 425 (2021) 131480.
6. D. S. Chauhan, M. A. Quraishi, V. Srivastava, J. Haque and B. E. ibrahimi, *J. Mol. Struct.*, 1226 (2021) 129259.
7. H. Wei, B. Heidarshenas, L. Zhou, G. Hussain, Q. Li and K. Ostrikov, *Mater. Today Sustain.*, 10 (2020) 100044.
8. B. E. A. Rani and B. B. J. Basu, *Int. J. Corros.*, 2012 (2012) 1.
9. L. Chen, D. Lu and Y. Zhang, *Materials*, 15 (2022) 2023.
10. E. E. Ebenso, C. Verma, L. O. Olasunkanmi, E. D. Akpan, D. K. Verma, H. Lgaz, L. Guo, S. Kaya and M. A. Quraishi, *Phys. Chem. Chem. Phys.*, 23 (2021) 19987.
11. A. Kokalj, M. Lozinšek, B. Kapun, P. Taheri, S. Neupane, P. Losada-Pérez, C. Xie, S. Stavber, D. Crespo, F. U. Renner, A. Mol and I. Milošev, *Corros. Sci.*, 179 (2021).
12. H. Lgaz and H. S. Lee, *Appl. Surf. Sci.*, 567 (2021) 150819.
13. L. Guo, C. Qi, X. Zheng, R. Zhang, X. Shen and S. Kaya, *RSC Adv.*, 7 (2017) 29042.
14. B. Aradi, B. Hourahine and T. Frauenheim, *J. Phys. Chem. A*, 111 (2007) 5678.
15. L. Guo, I. B. Obot, X. Zheng, X. Shen, Y. Qiang, S. Kaya and C. Kaya, *Appl. Surf. Sci.*, 406 (2017) 301.
16. N. Kovačević, I. Milošev and A. Kokalj, *Corros. Sci.*, 98 (2015) 457.
17. L. Guo, B. Tan, W. Li, Q. Li, X. Zheng and I. B. Obot, *J. Mol. Liq.*, 327 (2021) 114828.
18. L. Feng, S. Zhang, Y. Qiang, Y. Xu, L. Guo, L. Madkour and S. Chen, *Materials*, 11 (2018) 1042.
19. H. E. Aadad, M. Galai, M. Ouakki, A. Elgendy, M. E. Touhami and A. Chahine, *Surf. Interfaces*, 24 (2021) 101084.
20. L. Guo, M. Zhu, Z. He, R. Zhang, S. Kaya, Y. Lin and V. S. Saji, *Langmuir*, 38 (2022) 3984.
21. M. A. Deyab and Q. Mohsen, *Sci. Rep.*, 11 (2021) 21435.
22. A. HelmholtzSingh, K. R. Ansari, M. A. Quraishi, S. Kaya and L. Guo, *J. Nat. Gas Sci. Eng.*, 83

(2020) 103547.
23. B. E. Conway, J. O. M. Bockris and I. A. Ammar, *Trans. Faraday Soc.*, 47 (1951) 756.
24. M. Ramezanzadeh, G. Bahlakeh, B. Ramezanzadeh and Z. Sanaei, *J. Ind. Eng. Chem.*, 77 (2019) 323.
25. H. Erramli, O. Dagdag, Z. Safi, N. Wazzan, L. Guo, S. Abbout, E. Ebenso, C. Verma, R. Haldhar and M. E. Gouri, *Surf. Interfaces*, 21 (2020) 100707.
26. A. Mittal, L. Kurup and J. Mittal, *J. Hazard. Mater.*, 146 (2007) 243.
27. S. Qiu, W. Li, W. Zheng, H. Zhao and L. Wang, *ACS Appl. Mater. Inter.*, 9 (2017) 34294.
28. M. S. Walczak, P. Morales-Gil and R. Lindsay, *Corros. Sci.*, 155 (2019) 182.
29. A. E.-M. M, M. M. Shaban, M. A. Migahed and M. M. H. Khalil, *ACS Omega*, 5 (2020) 26626.
30. Q. H. Zhang, B. S. Hou, Y. Y. Li, G. Y. Zhu, Y. Lei, X. Wang, H. F. Liu and G. A. Zhang, *Chem. Eng. J.*, 424 (2021) 130519.
31. T. Le Minh Pham, T. Khoa Phung and H. Viet Thang, *Appl. Surf. Sci.*, 583 (2022) 152524.
32. N. Weder, R. Alberto and R. Koitz, *J. Phys. Chem. C*, 120 (2016) 1770.
33. Q. H. Zhang, Y. Y. Li, G. Y. Zhu, Y. Lei, X. Wang, H. F. Liu and G. A. Zhang, *Corros. Sci.*, 192 (2021) 109807.
34. L. Guo, Y. E. Bakri, R. Yu, J. Tan and E. M. Essassi, *J. Mater. Res. Technol.*, 9 (2020) 6568.
35. R. Solmaz, G. Kardas, M. Culha, B. Yazici and M. Erbil, *Electrochim. Acta*, 53 (2008) 5941